BILINGUAL PUBLISHING GROUP

Journal of Electronic & Information Systems

https://journals.bilpubgroup.com/index.php/jeis

ARTICLE

Seasonal Analysis of Real-Time Derived and ITU-R Modeled Surface Radio Refractivity in a Tropical Region Using a Low-Cost Developed Device

Abdulgafar Babatunde Giwa [1*] , ***Joseph Sunday Ojo*** [2], ***Opeyemi Vincent Omole*** [1], ***Waheed Ademola Toriola*** [3]

[1] *Department of Physics, Bamidele Olumilua University of Education Science and Technology, Ikere-Ekiti, Ikere-Ekiti P.M.B. 250, Nigeria*

[2] *Department of Physics, The Federal University of Technology Akure, Akure P.M.B. 704, Nigeria*

[3] *Department of Physics and Electronics, University of Ilesa, Ilesa P.M.B. 5089, Nigeria*

ABSTRACT

This study investigates seasonal and diurnal variations of surface radio refractivity in a tropical region by comparing real-time derived values from a low-cost automated Global System for Mobile Communication Signal Strength and Radio Climatological (GSM-RC) monitoring device with those modeled by ITU-R P.453-13. The GSM-RC device, installed at 3-m height, provided real-time, in-situ measurements of temperature, pressure, and humidity. Refractivity was derived in real-time from this high-resolution data and compared against model outputs across four months representing distinct climatic phases: January (dry season), April (commencement of rainy season), July (intense rainy season), and October (fading season). Results show a strong correlation between datasets, with seasonal atmospheric dynamics driving clear patterns. The dry season exhibited large diurnal fluctuations due to low humidity and high solar radiation, while the intense rainy season showed minimal variability from persistently high humidity and reduced temperature gradients. Transitional months displayed moderate instability. Although the ITU-R model provided reliable smoothed approximations, real-time derived data proved superior at capturing transient fluctuations, particularly during atmospheric instability. These

*CORRESPONDING AUTHOR:

A. B. Giwa, Department of Physics, Bamidele Olumilua University of Education Science and Technology, Ikere-Ekiti, Ikere-Ekiti P.M.B. 250, Nigeria; Email: giwa.abdulgafar@bouesti.edu.ng

ARTICLE INFO

Received: 21 January 2026 | Revised: 30 March 2026 | Accepted: 17 April 2026 | Published Online: 24 April 2026
DOI: https://doi.org/10.30564/jeis.v8i1.13026

CITATION

Giwa A.B., Ojo, J.S., Omole, O.V., et al. 2026. Seasonal Analysis of Real-Time Derived and ITU-R Modeled Surface Radio Refractivity in a Tropical Region Using a Low-Cost Developed Device. Journal of Electronic & Information Systems. 8(1): 80–96.
DOI: https://doi.org/10.30564/jeis.v8i1.13026

findings underscore the value of locally-sourced real-time data for capturing dynamic refractivity behaviour and highlight opportunities to enhance climatological propagation models. By linking observed patterns to West African monsoon phases, this work provides valuable insight for telecommunications system design, weather prediction, and regional atmospheric monitoring in tropical environments.

Keywords: Atmospheric Monitoring; In-Situ Measurement; ITU-R P.453-13; Radio Refractivity; Seasonal Variation; Tropical Region

1. Introduction

The complexity of tropospheric dynamics makes investigating surface refractivity particularly important in tropical environments. Since tropospheric conditions cannot be controlled, their variability and responses to different processes must be continuously monitored[1].

Surface refractivity is a key parameter in both radio wave propagation and meteorology, directly influencing signal transmission near the Earth's surface. It is therefore critical for applications such as radar systems, wireless communication networks, and weather forecasting, where accurate computation is essential for reliable system performance.

Refractivity can be determined using several approaches, including direct measurements with refractometers, estimation from meteorological parameters, radar measurements, and aerological soundings. For instance, Viher et al.[2,3] investigated multi-year refractivity profiles along the Adriatic coast using daily aerological soundings. More recently, radar-based refractivity estimation has gained increasing attention in the meteorological community[4]. Given this, atmospheric parameters are fundamental to the study of refractivity and anomalous propagation.

In Nigeria, several studies have examined surface refractivity. Scholars, including Oyinloye, Oyedum and Gambo, Falodun and Kolawale, Adeyemi and Ewetumo[5–8], used extrapolated radiosonde data to analyze gradients and variations. Despite methodological differences, their results consistently showed higher refractivity during the rainy season and lower values during the dry season. For example, Adeyemi and Kolawale[9] conducted in-situ measurements in Akure, concluding that humidity ("wet term") is the primary driver of both seasonal and diurnal refractivity variations.

Recent studies continue to reinforce the dominance of moisture in controlling surface refractivity in West Africa and other tropical environments. Tanko et al.[10] reported that regions within the rainforest and coastal climatic zones exhibit significantly higher surface refractivity than inland and semi-arid regions, with refractivity peaks occurring concurrently with periods of intense rainfall. Similarly, Ladan et al.[11] showed that mean refractivity values during the rainy season are substantially higher than during the dry season in north-western Nigeria, and confirmed that relative humidity is the principal driver of both seasonal and diurnal refractivity variability.

Falodun and Ajewole[12,13] used automatic weather station (AWS) sensors at 0 m and 100 m to investigate refractivity fluctuations in the lower troposphere in Akure South, southwestern Nigeria. Their results confirmed that refractivity is strongly influenced by local climatic conditions and is typically lowest around local noon and highest at night or in the early morning, which is a pattern driven by solar insolation, temperature, and humidity cycles. Kolawale and Owonubi[14] also found that coastal regions across Africa typically exhibit higher surface refractivity.

A consistent conclusion from these works, including those along the Adriatic coast[3,15,16], is that refractivity is lower during the day and higher at night, and that coastal regions experience enhanced values.

However, determining surface refractivity accurately remains challenging. Issues include uncertainties in data availability and quality, such as gaps in monitoring networks, instrumentation errors, and limited spatiotemporal resolution, as well as simplifications inherent in climatological models[17]. These models may neglect non-linear interactions and depend on input parameters (temperature, humidity, pressure) that themselves contain uncertainty.

Therefore, real-time, in-situ measurements are essential for capturing rapid atmospheric changes and providing a reliable benchmark. They offer higher accuracy, superior temporal resolution, and better spatial fidelity than model-derived estimates, minimizing errors associated with model

assumptions[18]. Recent advances have applied machine learning for radio refractivity prediction across diverse climatic zones in West Africa, with models such as LightGBM and LSTM showing improved predictive skill over traditional atmospheric models[19].

The growing interest in real-time and low-cost monitoring platforms is further motivated by recent developments in radio-climatological sensing systems. Ukhurebor and Nwankwo[20] demonstrated that integrated and low-cost GSM-based monitoring devices can provide concurrent measurements of meteorological parameters and radio signal characteristics suitable for propagation and refractivity studies, thereby improving temporal resolution and data availability in data-sparse regions.

This study addresses a gap in prior Nigerian research by moving beyond reliance on radiosonde or model-interpolated data. We employ a novel, low-cost GSM-RC device developed by Giwa et al.[18] to collect continuous, high-resolution in-situ meteorological data. The primary objectives are to: (1) perform a comparative seasonal analysis of real-time derived refractivity against values modeled by the ITU-R P.453-13 standard; (2) characterize the impact of seasonal variations, explicitly linked to the West African monsoon, on refractivity dynamics; and (3) evaluate the implications of real-time data for precision-critical applications in telecommunications and atmospheric monitoring. This work aims to provide a robust platform for improved network design and policy formulation in the region.

2. Theoretical Background

The International Telecommunication Union (ITU-R) recommends calculating the atmospheric refractive index, *n*, using the formulation of Bean and Dutton[21], which provides a standardized approach for refractivity estimation.

Under typical conditions near the Earth's surface, the refractive index *n* is approximately 1.003[22]. The corresponding refractivity, denoted as *N*, quantifies radio wave refraction in the troposphere, as given in Equation (1).

$$N = (n-1) \times 10^{-6} \tag{1}$$

where "*N*" denotes radio refractivity and "*n*" determines the air's refractive index. Variations in weather conditions can distort radio waves during atmospheric transmission[23–25]. This effect is described mathematically in Equation (2).

$$N = N_{dry} + N_{wet} = 77.6\frac{P}{T} + 3.75 \times 10^5 \frac{e}{T^2} \tag{2}$$

where "*T*" is the Temperature in kelvin, "*P*" is the atmospheric pressure in hectopascal. And "*e*" is water vapour pressure in hectopascal.

Equation (3) converts temperature from Celsius to Kelvin:

$$T(K) = 273.15 + t(^\circ C) \tag{3}$$

The saturation vapour pressure, usually expressed in hPa, represents the vapour pressure in fully saturated air. It can be evaluated using several methods. Equation (4) estimates saturation vapour pressure from the water vapour partial pressure (e_s) and relative humidity (*H*, %):

$$e = \frac{H \times e_s}{100} \tag{4}$$

The Clausius–Clapeyron relation (Equation (5)) can also be used to compute the saturation vapour pressure (e_s):

$$e_s = 6.11 exp^{\left[\frac{17.26(T-273.16)}{T-35.67}\right]} \tag{5}$$

e_s is the saturated water vapour pressure, and "*T*" is the temperature in kelvin. The conditions listed in (6) can be used to generate the refractivity profile.

$$M = N(z) + 0.157z \tag{6}$$

Radio refractivity (*N*) reflects the influence of meteorological parameters at the Earth's surface. It can be expressed as *M(z)*, where *z* represents height in meters above the ground.

3. Methodology

3.1. Instrumentation

This study is based on a high-resolution, time-synchronised dataset of the essential meteorological parameters required for calculating radio refractivity. Data were acquired using a custom-developed, low-cost GSM-RC (Global System for Mobile Communication Signal Strength and Radio Climatological) automated device; its design and validation are detailed by Giwa et al.[18]. Recent GSM-based radio-climatological monitoring systems have also been shown to be effective for combined atmospheric and radio-propagation studies, particularly for continuous and low-cost deployments in tropical environments[20].

The GSM-RC device's integrated design is particularly valuable as it solves the critical problem of asynchronous data acquisition. Accurate concurrent measurement of temperature (T), atmospheric pressure (P), and relative humidity (RH) at a single point is essential for refractivity analysis. The device consolidates these sensors into one portable package, eliminating the synchronisation errors inherent in using separate instruments.

The core sensing subsystem consists of a BME280 sensor that measures temperature (range: −40 °C to +85 °C; accuracy: ±2 °C) and pressure (range: 300–1,100 hPa) and an HTU31 sensor for measuring relative humidity. An Arduino ATmega 2560 microcontroller orchestrates the system, polling these sensors at programmed intervals. For the specific purpose of this refractivity analysis, a dedicated computational subsystem was implemented. This subsystem, centred on the same Arduino microcontroller, is programmed to apply the standard refractive index formula in real-time to the incoming T, P, and RH data streams. The design of this calculation subsystem, illustrating the data flow from sensors to refractivity output, is presented in the circuit diagram (**Figure 1**), while the GSM-RC measuring device is presented in the diagram (**Figure 2**). All raw and processed data, including the real-time derived refractivity (N), GPS-derived location, and timestamps, are stored locally on a micro-SD card, ensuring data integrity during field deployment. Prior to its use in this study, the device's meteorological outputs had a rigorous validation against a standard Vantage Pro weather station in a co-located setup.

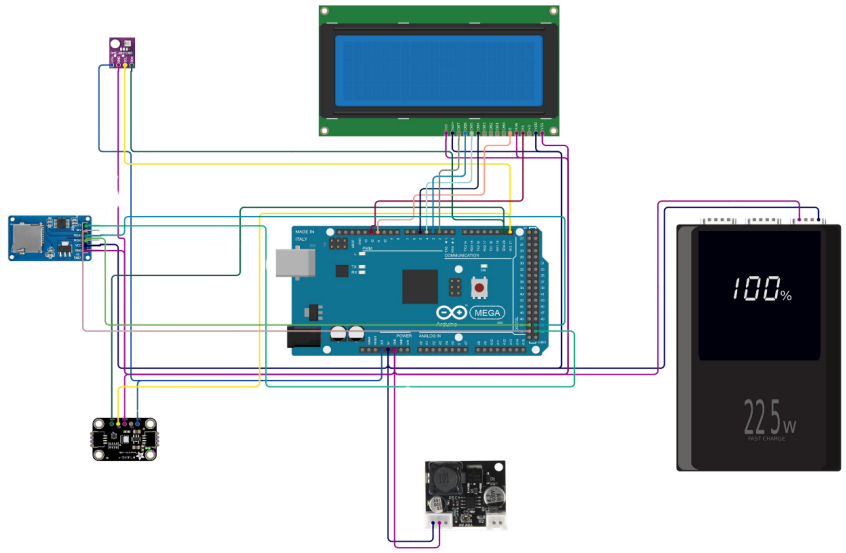

Figure 1. Circuit diagram of the computation subsystem of the adopted device.

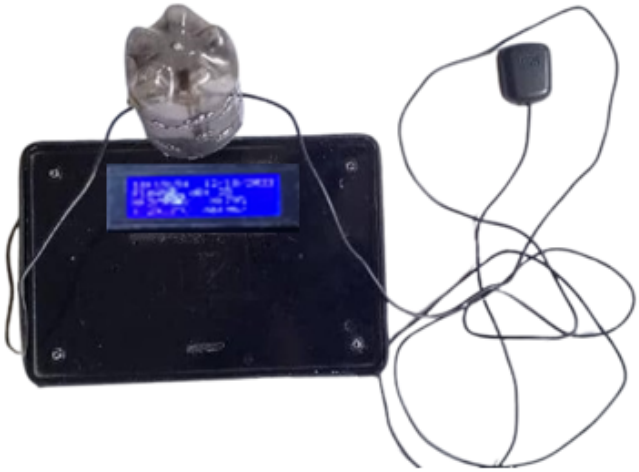

Figure 2. The GSM-RC.

For this study, the validated device and its dedicated refractivity subsystem were deployed to collect continuous measurements. This setup directly yields the real-time derived refractivity (N) value that serves as the reference dataset against which the model-predicted refractivity from the ITU-R P.453 recommendation is compared.

3.2. Data and Climate of the Study Area

Tropospheric surface refractivity data were collected continuously from January to December 2025 at the study site, with measurements recorded hourly (00:00 AM–23:00 PM). The primary data streams were: (1) high-resolution in-situ measurements of temperature (°C), relative humidity (%), and pressure (hPa) from the GSM-RC device; and (2) refractivity values in N-units directly logged by the device's onboard computational subsystem. From these co-located meteorological measurements, two refractivity datasets were generated for comparative analysis. Locally derived refractivity (N-Derived) was calculated in real-time by the GSM-RC device using the standard ITU-R formula. In parallel, modeled refractivity (N-Modeled) was generated by applying the same hourly Temperature, Pressure, and Relative Humidity data as input to the ITU-R P.453-13 model.

For analysis, the year was divided into four representative months: January (dry season), April (commencement of rainy season), July (intense rainy season), and October (fading season). The measured refractivity data were first filtered and compared with values reported in the literature. Seasonal and solar influences were then analysed to assess their impact on refractivity fluctuations.

The study site is Akure, the capital of Ondo State, Nigeria. It is bordered by Owo to the east, Akure North/Ifedore to the north, Ile-Oluji/Oke-Igbo to the west, and Idanre to the south. Akure has a humid tropical climate typical of southwestern Nigeria, strongly influenced by dry northeasterly winds from the Sahara (harmattan) and moist southwesterly monsoon winds from the Atlantic. Two main seasons prevail: a rainy season (April–October, with a short August break) and a dry season (November–March). According to Ojo et al. [26], Akure is in the P-zone of the ITU-R rain climatic zoning and receives an average of 1485.57 mm of rainfall per hour. Temperatures range from about 22 °C in December–February to 32 °C in March. The River Ala and its tributaries drain the surrounding rainforest vegetation [27]. Weather variability in Akure has also been described as highly unpredictable and chaotic [28]. **Figure 3** shows the geography of the experimental site at the Federal University of Technology Akure, in Ondo State.

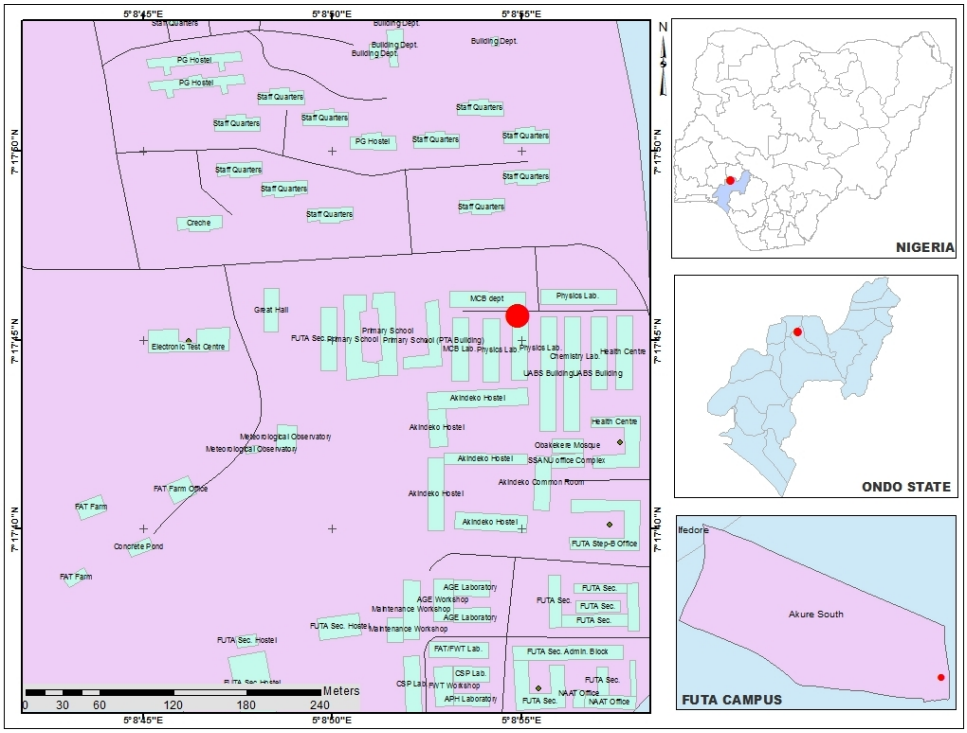

Figure 3. Map of Ondo State, Federal University of Technology Akure, showing the experimental site.

3.3. Statistical Analysis

Validating the Device Measurement with Existing Equipment

The GSM-RC device was validated against a Davis Vantage Vue Integrated Sensor Suite (ISS) installed at the Federal University of Technology, Akure. Both instruments were co-located and configured to record temperature, pressure, and relative humidity at one-minute intervals. Data were logged independently and later analysed. To minimize bias, the GSM-RC sensors were housed in a prototype Stevenson screen. Validation results are presented in **Figures 4–6** and characterized by Equations (7)–(9).

For Temperature (BME280),

$$T_p = 0.7624T_m + 17.0991 \tag{7}$$

For RH,

$$\mathrm{RH}_p = 0.6433\mathrm{RH}_m + 16.489 \tag{8}$$

For Pressure,

$$P_p = 0.5275P_m + 498.38 \tag{9}$$

where T_p, RH_p and P_p are the predicted temperature, relative humidity and pressure, while T_m, RH_m and P_m are the measured temperature, relative humidity and pressure. A correlation analysis was conducted, resulting in a correlation coefficient of 0.83 for relative humidity, 0.98 for temperature, and 0.95 for pressure between the developed and standard devices.

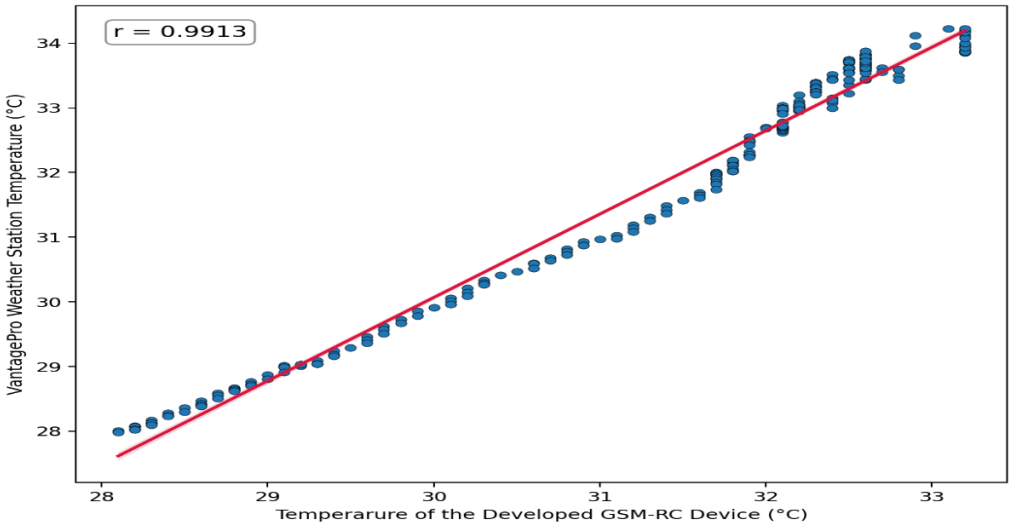

Figure 4. The correlation of the temperature for the GSM-RC Device with the VantagePro Weather Station.

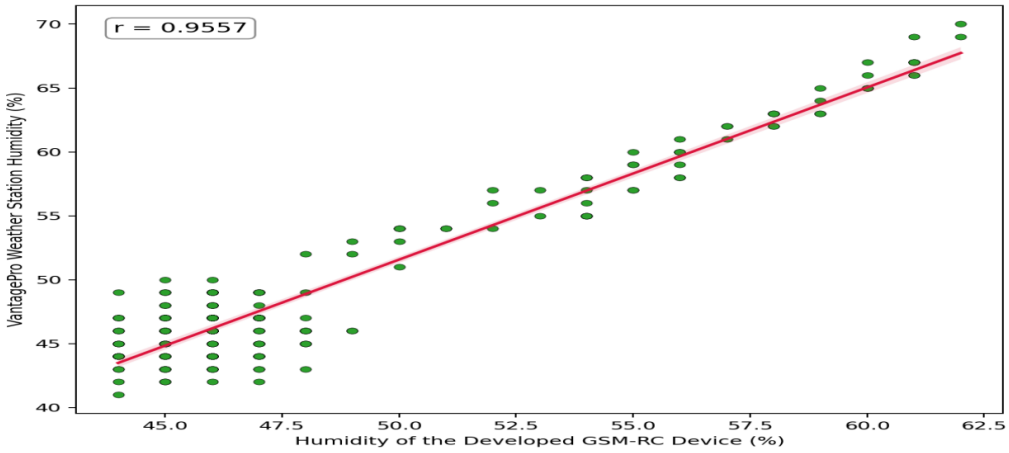

Figure 5. The correlation of the relative humidity of the GSM-RC Device with the VantagePro Weather Station.

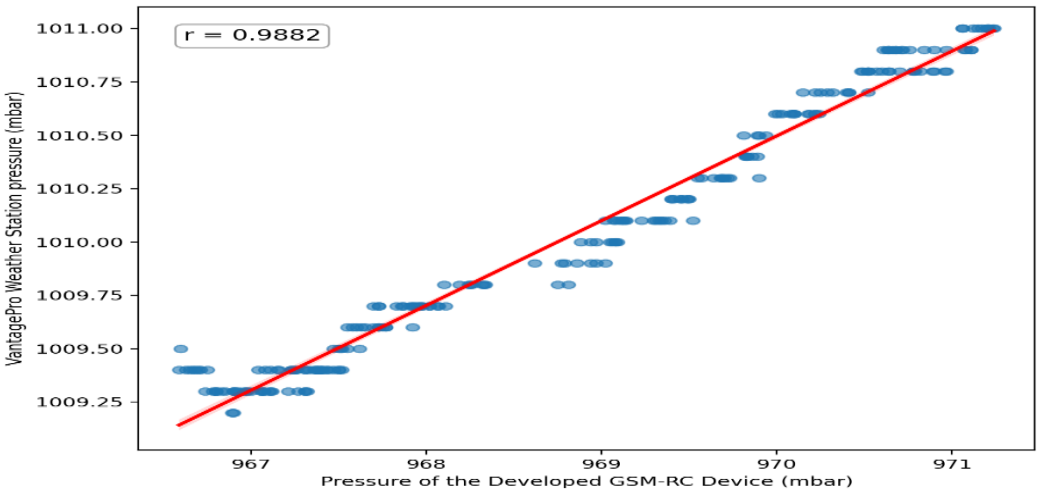

Figure 6. The correlation of the pressure for the GSM-RC Device with the VantagePro Weather Station.

3.4. Statistical Validation

To prove the validity of the analytical method, statistical analysis of the data collected during the validation was also presented. The computation of the correlation (R^2), root mean square error (RMSE), mean absolute error (MAE), and standard deviation (S.D) are the main variables utilised for the interpretation of the results of analytical technique validation.

The correlation (R^2) was used to assess the strength of the linear relationship between the two datasets. A higher R^2 value indicates that the GSM-RC device readings closely follow the trend of the VantagePro data, suggesting strong agreement in their response patterns. Correlation (R^2) was calculated:

$$R^2 = 1 - \frac{RSS}{TSS} \tag{10}$$

where R^2 is the coefficient of determination, RSS is the sum of squares residual and TSS is the total sum of squares.

The Root Mean Square Error (RMSE) provides a measure of the average magnitude of error between the two devices. It is particularly sensitive to larger deviations. Lower RMSE values indicate that the GSM-RC readings are more accurate and closely match those of the VantagePro. The RMSE was calculated using:

$$RMSE = \sqrt{\frac{\sum (x_i - \widehat{x}_i)^2}{N}} \tag{11}$$

where RMSE is the root mean square error, x_i is the actual observation of time series, $\widehat{x}_i$ is the estimated time series and N is the number of non-missing data points.

Mean Absolute Error (MAE) reflects the average absolute differences between the readings from the two devices, offering a straightforward interpretation of how much, on average, the GSM-RC deviates from the VantagePro. The MAE was also calculated using:

$$MAE = \frac{\sum |y_i - x_i|}{n} \tag{12}$$

where MAE is the mean absolute error, y_i is the prediction, x_i is the true value and n is the total number of data points.

Standard Deviation (S.D) was used to evaluate the variability in the differences between the two sets of measurements. A lower S.D implies that the GSM-RC device demonstrates more consistent performance when compared to the VantagePro, with less fluctuation in its measurement error.

The standard Deviation (S.D) was calculated using:

$$S = \sqrt{\frac{\sum (x_i - \overline{x})^2}{n-1}} \tag{13}$$

where x_i is the actual observation, $\overline{x}$ is the mean and n is the total number of observations.

A statistical software programme was used to carry out these calculations. **Table 1** shows the results obtained from the statistical validation of the radio climatological parameters between the VantagePro weather station and the developed device.

Table 1. Statistical validation of measured data for Radio climatological parameters between the developed GSM-RC device and the Standardized VantagePro.

Parameters	R^2	RMSE	MAE	S.D
Temperature (T)	0.983	0.181	2.499	3.144
Relative Humidity (RH)	0.832	0.350	5.391	9.994
Pressure (P)	0.957	1.917	4.917	1.554

3.5. Data Quality Control

Quality control procedures were applied to ensure the reliability of measurements. Data were screened for missing or inconsistent values, and spurious readings caused by sensor malfunction or transmission errors were removed. Outliers were identified using threshold limits (e.g., relative humidity >100% or negative values) and excluded from analysis. To minimize short-term noise, one-minute raw data were aggregated into hourly averages prior to analysis.

3.6. Comparative Analysis with Existing Methods

A comparative analysis was conducted to evaluate the GSM-RC device against established refractivity measurement methods reported in the literature. **Table 2** presents this comparison across multiple performance criteria.

The GSM-RC device achieves accuracy comparable to standard AWS (R^2 = 0.98 for temperature, 0.95 for pressure, 0.83 for RH) at approximately 3% of the cost. This dramatic cost reduction enables dense sensor network deployment impossible with conventional methods. The device's continuous 1-minute sampling provides superior temporal resolution compared to twice-daily radiosondes or daily satellite products, proving essential for capturing rapid diurnal fluctuations (78.76 N-units range in January) and transitional instability missed by coarser sampling. Real-time onboard refractivity calculation eliminates post-processing delays, enabling immediate data availability for time-sensitive applications. The integrated sensor design ensures perfect synchronization of meteorological measurements, eliminating errors inherent in separate instruments. The GSM-RC device is ideally suited for long-term monitoring networks, high-resolution diurnal studies, educational applications, and ground-truth validation of satellite products in resource-constrained settings.

Table 2. Comparative Analysis of Refractivity Measurement Methods.

Method	Accuracy	Cost	Temporal Resolution	Spatial Coverage	Deployment Complexity	Real-Time Processing
GSM-RC Device	High	Low ($150)	Continuous (1-min)	Point	Low	Yes
Radiosonde	Very High	High ($300–500/launch)	Twice daily	Vertical profile	High	No
Automatic Weather Station	High	Medium-High ($2,000–5,000)	Continuous	Point	Medium	Usually no
Satellite-derived	Medium	Low	Daily-weekly	Regional/Global	Low	No
Radar-based	Medium-High	Very High ($100,000+)	Continuous	Local area	Very High	Yes
Refractometer	Very High	Very High ($20,000–50,000)	Continuous	Point	High	Yes

4. Results and Discussion

4.1. Seasonal Analysis of the Measured Refractivity Data and the Estimated Refractivity Data

This section presents a seasonal analysis of tropospheric surface refractivity, comparing values derived from the GSM-RC device with those modeled by the ITU-R P.453-13 standard. To examine the influence of seasonal atmospheric conditions, hourly refractivity values were averaged and analysed. Four months were selected to represent the dominant climatic regimes of the West African monsoon system: January (dry season), April (commencement of the rainy season), July (intense rainy season), and October (fading rainy season). A statistical comparison between locally derived refractivity (N-Derived) and modeled refractivity (N-Modeled) was conducted to assess seasonal variability and model performance under these differing atmospheric conditions. All graphical analysis and figure generation were performed using Python software.

4.2. Influence of Dry Season (January) on the Refractivity Values

The real-time refractivity data were analysed over a 24-h cycle using daily observations. The dataset from 01/01/2025 was selected because it demonstrates correlation characteristics consistent with those of the full dataset.

The diurnal pattern for January (**Figure 7**) shows that both real-time derived (N-Derived) and modeled (N-Modeled) refractivity follow a pronounced wave-like trend. Values peak in the early morning (e.g., N-Derived: 335.91–341.83 N-units), decrease significantly by midday (N-Derived: 263.15 N-units), and recover through the evening (N-Derived: 330.28 N-units). While the N-Modeled data captures this general pattern, it provides a smoothed approximation of the fluctuations.

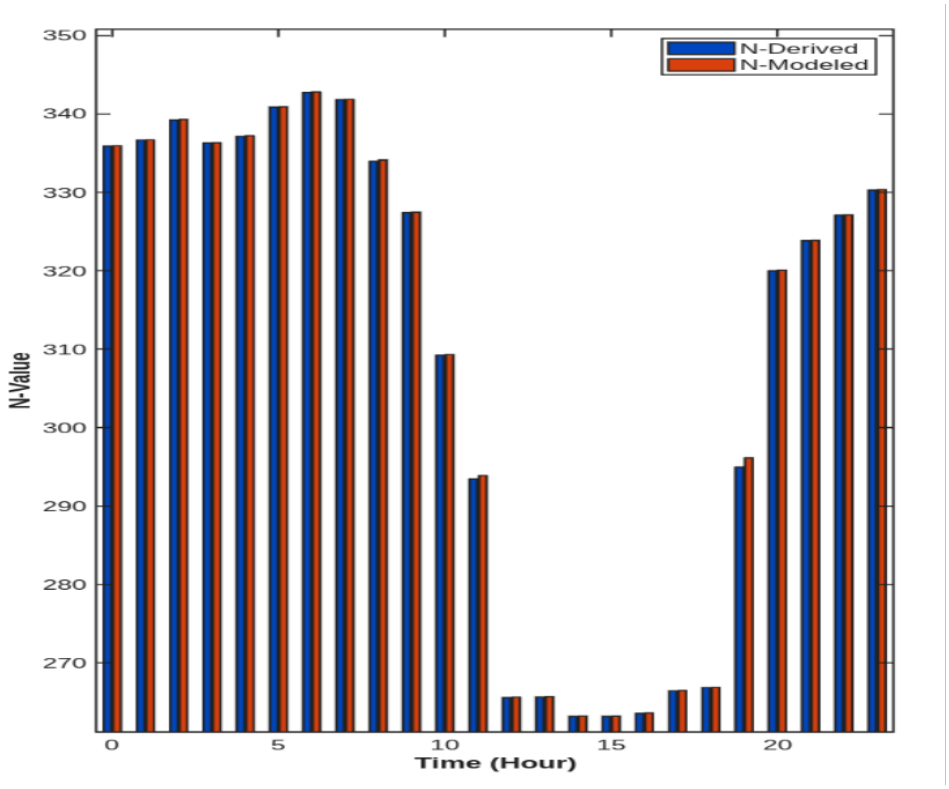

Figure 7. Mean hourly variation of Derived and Modeled Refractivity values on a typical day (01-01-2025).

This pattern is characteristic of the dry season, driven by low humidity and high solar radiation, which leads to minimum refractivity at midday when temperatures peak and humidity is lowest[29,30]. The significant diurnal fluctuation is a well-documented feature of dry seasons, resulting from clear skies and strong temperature gradients[31,32]. A similar dry-season behaviour, characterised by pronounced daytime minima and night-time maxima in surface refractivity, has been reported in recent tropical studies, where reduced atmospheric moisture and enhanced daytime heating were identified as the dominant physical drivers[11]. Recent measurements over Bauchi revealed distinct seasonal refractivity peaks and indicated that wet-season humidity contributes heavily to refractivity variations, confirming the importance of atmospheric moisture in propagation studies[33].

The physical mechanism follows the Clausius-Clapeyron relation, where rising temperatures during the day decrease the concentration of atmospheric water vapor. This lowers the air's dielectric constant, causing the pronounced midday dip in refractivity. Conversely, radiative cooling at night increases humidity near the surface, leading to the morning and evening peaks. The locally derived data (N-Derived) accurately captures these rapid, physically driven changes, while the ITU-R model output (N-Modeled) delivers a climatologically smoothed representation.

Table 3 shows a nearly perfect positive correlation (0.99997) between real-time derived and modeled refractivity

data, indicating the model's accuracy in predicting refractivity. The Root-Mean-Square-Error (RMSE) of 0.333810251 represents the average size of errors between the derived Refractivity and modeled Refractivity data, showing minimal deviation with a value of 0.33. The Mean Absolute Error (MAE) of 0.111429283 displays the average absolute difference between observed and estimated values, confirming minimal discrepancies with a low MAE of 0.11.

Table 3. Statistical analysis between N-derived and the N-modeled refractivity during the Dry Season.

Correlation	RMSE	MAE	R^2	Percentage Error
0.99997	0.33381	0.11143	0.99994	0.00826

Additionally, the determinant (R^2) correlation of 0.99994 demonstrates that the computed values account for 99.994% of the variation in derived refractivity, validating the model's fit and reliability. The Percentage Error of 0.00826 indicates a very low error percentage, further supporting the excellent alignment between the derived Refractivity and modeled Refractivity data. Overall, the model is essentially error-free based on these results.

4.3. Influence of Commencement of Rainy Season (April) on the Refractivity Values

The diurnal trend for April on 01/04/2025 (**Figure 8**) shows that both real-time derived (N-Derived) and modeled (N-Modeled) refractivity follow a stabilized wave-like pattern. Values are relatively high in the early morning (e.g., N-Derived: 300.27–309.25 N-units), exhibit a minor decrease at midday (N-Derived: 266.42 N-units), and stabilize in the evening (N-Derived: 328.41 N-units). The N-Modeled data closely follow this trend with minimal deviation. In comparison to January, the datasets show better alignment and fewer discrepancies.

This pattern reflects the onset of the rainy season, characterized by increasing atmospheric moisture and cloud cover. The higher humidity mitigates the effect of temperature-driven variations in refractivity, making the midday dip less pronounced than in the dry season. Increased cloud cover moderates solar radiation, further reducing diurnal temperature gradients and leading to smoother refractivity patterns [34–36]. Studies on coastal refractivity gradients in Nigeria demonstrate that wet season refractivity values are significantly higher than dry seasons and that refractivity gradients and effective Earth radii vary across climatic zones, influencing propagation conditions [37].

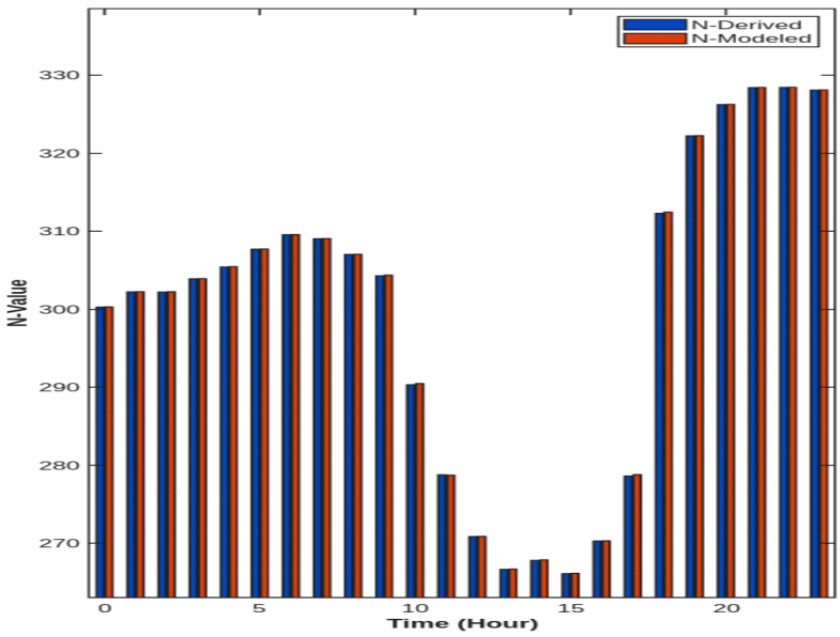

Figure 8. Mean hourly variation of Derived and Modeled Refractivity values on a typical day (01-04-2025).

Physically, the rising moisture increases the air's dielectric constant, enhancing refractivity. This aligns with Dalton's Law of Partial Pressures, where the total atmospheric refractivity increases with the partial pressure of water vapour. While the modeled data (N-Modeled) provides a reliable approximation under these stabilizing conditions, the locally derived data (N-Derived) more precisely capture the residual diurnal distinctions.

Table 4 indicates an almost perfect relationship between the derived and modeled refractivity data, with the correlation (0.999997) being higher than in January. The RMSE (0.176452225) is reduced as compared to January, which implies that the model's predicted accuracy is even better in April. Also, the MAE (0.031135388) has a substantially lower value; this shows that the variations between observed and calculated values are minimal. The R^2 (0.99999) implies that practically all variability in the derived data is represented by the modeled values, further validating the model's resilience. The extremely low percentage error (0.01037) indicates that the values are strongly aligned.

Table 4. Statistical analysis between the N-derived and the N-modeled refractivity data during the Commencement of the rainy season.

Correlation	RMSE	MAE	R^2	Percentage Error
0.99997	0.176452225	0.031135388	0.99999	0.01037

4.4. Influence of Intense Rainy Season (July) on the Refractivity Values

Figure 9 illustrates that during July (01/07/2025), both real-time derived (N-Derived) and modeled (N-Modeled) refractivity show exceptionally stable values with minimal diurnal variation. N-Derived values remain within a narrow range (e.g., 364.62 to 368.14 N-units), and N-Modeled data closely mirror this near-flat trend.

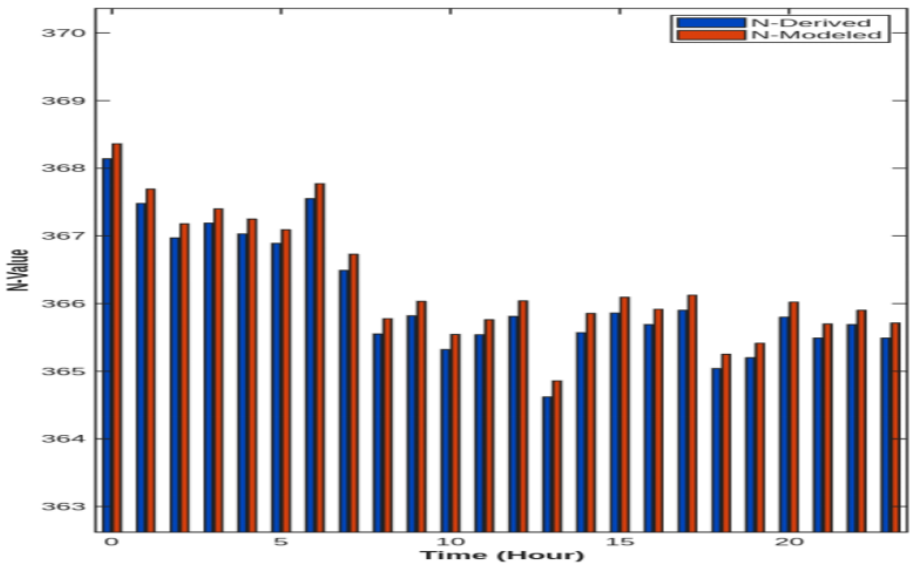

Figure 9. Mean hourly variation of Derived and Modeled Refractivity values on a typical day (01-07-2025).

This high stability is a hallmark of the intense rainy season, characterized by persistent cloud cover, regular rainfall, and consistently high atmospheric moisture. These conditions minimize solar heating and reduce thermal gradients, effectively suppressing the diurnal temperature cycle that drives refractivity variations in drier months [30,34,36]. Comparable refractivity stabilisation during the peak rainy season has recently been reported over tropical and subtropical regions, where persistently high humidity and cloud cover suppress diurnal variability in near-surface refractivity [10].

The physical basis for this lies in the dominance of the wet term of the refractivity equation. The high and constant concentration of water vapor significantly increases the atmosphere's dielectric constant, as described by the principles

governing electromagnetic wave propagation. Consequently, refractivity is elevated and stabilized, resulting in the observed nearly flat diurnal profile.

Under these stable atmospheric conditions, the ITU-R model (N-Modeled) performs well, providing a smoothed representation that aligns closely with the general trend. However, the derived data (N-Derived) retains the capacity to capture subtle, real-time fluctuations that may result from transient weather disturbances within the prevailing moist regime.

The stability of refractivity during this season emphasises the importance of humidity in controlling refractivity values and atmospheric dielectric characteristics. Although the correlation (0.999847) in **Table 5** remains extremely high, it is slightly lower than in January and April, indicating minor alignment deviations during this time. A higher RMSE (0.468317) compared to previous months suggests more differences between the derived and modeled refractivity data. The MAE (0.219321) indicates greater average discrepancies between the derived and modeled data, possibly influenced by seasonal or environmental factors. Nevertheless, the R^2 value of 0.99969 remains excellent, showing that the calculated model explains almost all of the variation in the measured refractivity.

Table 5. Statistical analysis between N-derived and the N-modeled refractivity during the intense rainy season.

Correlation	RMSE	MAE	R^2	Percentage Error
0.999847	0.468317	0.219321	0.99969	0.05957

4.5. Influence of Fading Season (October) on the Refractivity Values

Figure 10 shows that during October on 01/10/2025, both real-time derived (N-Derived) and modeled (N-Modeled) refractivity exhibit renewed diurnal variability, markedly greater than the stable pattern observed in July. N-Derived values, for instance, range from 370.35–371.96 N-units in the morning, drop to 368.72 N-units in the afternoon, and recover slightly to 368.85 N-units in the evening. The N-Modeled data follows this general trend but presents a more smoothed distribution of the fluctuations.

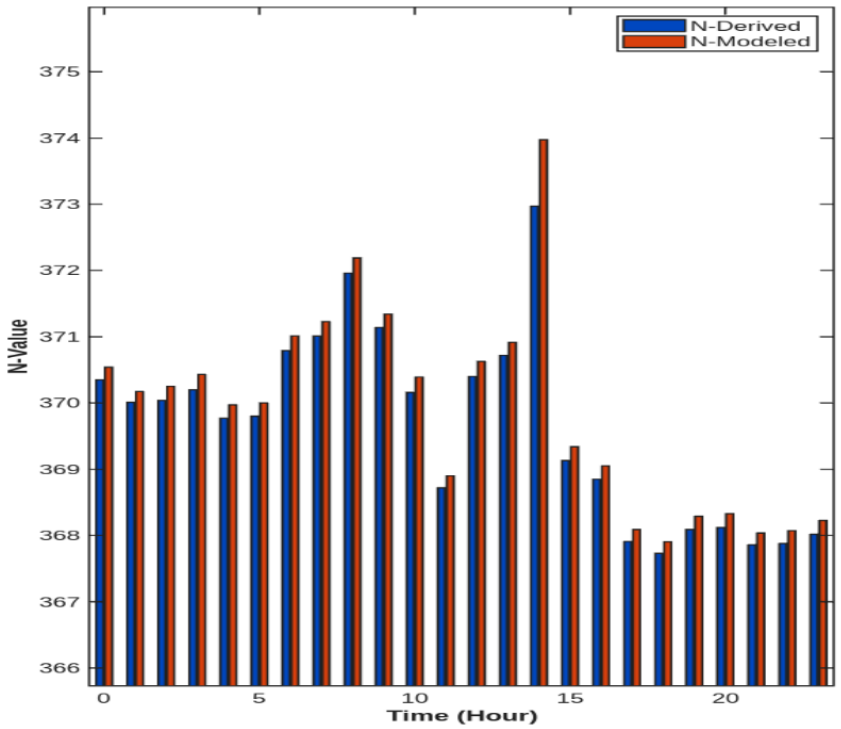

Figure 10. Mean hourly variation of Derived and Modeled Refractivity values on a typical day (01-10-2025).

This period marks the transition from the rainy season back to drier conditions, characterized by inconsistent moisture levels, fluctuating solar radiation, and increasing thermal instability. The retreat of consistent cloud cover allows for uneven surface heating, which can create rising air currents and convective activity that disrupt stable atmospheric stratification.

These dynamic conditions intensify refractivity changes, particularly around midday. The physical mechanism follows the Clausius-Clapeyron relation, where rising temperatures coupled with decreasing humidity lead to a more pronounced diurnal cycle in atmospheric water vapor content, and consequently, in refractivity. This increased variability during transitional seasons is well-documented [11].

The derived data (N-Derived) better capture these rapid, instability-driven changes. In contrast, the ITU-R model output (N-Modeled), which relies on climatological averaging, tends to smooth over this variability. This contrast underscores the challenge for models during dynamically unstable periods and highlights the critical importance of real-time, in-situ measurements for accurately resolving rapid atmospheric changes.

Although the correlation for October (**Table 6**) remained strong (0.995898), it was the lowest among the four seasonal periods. This indicates that the derived and modeled refractivity data in October were somewhat out of alignment. The RMSE (0.434962) also showed larger differences between the derived and modeled refractivity data, similar to what was seen in July. Compared to previous months, the relatively high MAE (0.189192) suggests more significant disparities.

Table 6. Statistical analysis between N-derived and the N-modeled refractivity during the fading season.

Correlation	RMSE	MAE	R^2	% Error
0.995898	0.434962	0.189192	0.99181	0.05108

It appears that the computed model may not accurately account for as much variance in October as it does in other months, despite the still strong R^2 value (0.99181). In comparison to January and April, the error percentage was higher (0.05108), indicating that the model's accuracy was lower in this particular month.

4.6. Effect of the Seasonal Variations on the Measured Tropospheric Surface Refractivity Data and Calculated Tropospheric Surface Refractivity Data

The analysis reveals that the ITU-R modeled refractivity shows degraded performance during months of significant atmospheric transition, particularly the peak and fading rainy seasons (July and October), as evidenced by higher RMSE, MAE, and Percentage Error values (**Tables 5** and **6**). This aligns with findings that irregular seasonal conditions lead to increased refractivity estimation errors, whereas stable periods yield lower discrepancies [38]. This indicates that the ITU-R P.453-13 model, while reliable in steady states, does not fully resolve the complex interplay of rapidly shifting environmental variables, such as temperature, humidity, and pressure that define these dynamic periods. Such limitations in capturing extreme or transitional conditions are a recognized challenge for climatological models [39]. Recent comparative assessments have further shown that standard refractivity models, including ITU-based formulations, tend to underestimate near-surface refractivity and refractivity gradients under highly humid and convective tropical conditions [40].

Consequently, for applications demanding high precision and real-time responsiveness such as telecommunications network optimization during severe weather or detailed atmospheric research, refractivity derived from local in-situ measurements is strongly recommended. Machine-learning-based refractivity estimation has also been explored, showing that models trained on multi-parameter meteorological data can outperform simpler regression models, particularly across contrasting coastal and inland sites [41].

Recent studies have demonstrated that high-frequency and non-traditional sensing approaches can successfully resolve short-term atmospheric moisture fluctuations that directly influence refractivity. For example, Sakkas et al. [42] showed that mobile communication signal measurements can be used to infer atmospheric humidity and refractivity variability with strong correlation, highlighting the importance of dense and continuous monitoring for capturing rapid atmospheric changes.

This locally derived data inherently captures real-time

atmospheric fluctuations, providing an accuracy that model-based estimations cannot match under dynamic conditions. While modeled data remain valuable for long-term trend forecasting or where direct measurements are absent, their application during volatile periods requires validation against local, ground-truth data.

Crucially, the observed refractivity variations are not merely local sensor readings but a reflection of macro-scale climatology. The diurnal and seasonal patterns align coherently with the advance, peak, and retreat of the West African monsoon. The large diurnal fluctuations in January are driven by dry Harmattan northeasterlies, while the stabilized refractivity in July results from persistent moisture-laden southwesterly monsoon winds. The transitional instability in April and October corresponds to the inter-phase shifts of the monsoon system. Seasonal refractivity modeling in Jos further supports the strong wet/dry seasonal contrast observed in our dataset, and highlights the potential for improved prediction through climatic regression techniques [43].

This explicit link to monsoon dynamics underscores the climatological significance of the findings: monitoring locally derived refractivity provides a valuable, high-resolution record of regional atmospheric processes, essential for both applied engineering and climate studies.

5. Future Scope

1. **Regional Network Expansion:** Deploying multiple GSM-RC devices across West Africa would enable spatial mapping of refractivity fields across different climatic zones such as coastal, rainforest, savanna, and Sahel, capturing the full spectrum of atmospheric dynamics affecting radio propagation.
2. **Machine Learning Integration:** High-resolution refractivity data can train neural networks and LSTM models for predictive forecasting. Such capabilities would enable adaptive modulation and power control in telecommunication systems based on anticipated propagation conditions.
3. **Vertical Profile Characterization:** Installing sensor arrays at heights of 3 m, 10 m, 30 m, and 50 m would characterize refractivity gradients essential for predicting ducting, super-refraction, and beyond-line-of-sight propagation.
4. **Long-term Climatological Analysis:** Continuous measurements over 5-10 years would establish baseline refractivity statistics and detect climate change impacts on propagation conditions, serving as an early warning for shifts in monsoon timing or intensity.
5. **IoT Integration:** Connecting GSM-RC devices to cloud platforms would enable real-time data accessibility for telecommunications optimization, aviation nowcasting, and public awareness through web and mobile applications.
6. **Model Enhancement:** The dataset can inform region-specific corrections to the ITU-R P.453-13 model, particularly for transitional seasons (April, October), where current performance shows limitations, potentially informing future ITU-R recommendations.
7. **Application-Specific Studies:** Correlating refractivity with actual GSM signal strength would establish quantitative relationships between atmospheric conditions and propagation effects, enabling fade mitigation and dynamic power control strategies.
8. **Numerical Weather Prediction:** Assimilating high-resolution refractivity data into NWP models could improve forecast accuracy for convective events and monsoon dynamics dependent on atmospheric stability and moisture distribution.
9. **Sensor Development:** Next-generation improvements could include solar-powered operation, multi-height measurement capability, additional sensors (rainfall, wind), and enhanced accuracy through improved calibration procedures.
10. **Educational Applications:** The low-cost, open-source design provides hands-on training opportunities for students in atmospheric science and telecommunications engineering, building local expertise and reducing dependence on external technical support.

Recent large-scale analyses have shown that long-term refractivity and rainfall datasets can be effectively combined to support data-driven prediction of atmospheric propagation conditions across multiple urban locations [44].

6. Conclusions

This study provides a comparative seasonal analysis of radio refractivity in a tropical West African region, con-

trasting values derived from local in-situ measurements with those modeled by the ITU-R P.453-13 standard. The results demonstrate that while the model provides reliable approximations under stable atmospheric conditions, refractivity derived from local, real-time meteorological data is superior for capturing dynamic variability, particularly during periods of significant atmospheric transition as observed in the wet-dry seasonal transitions.

Therefore, for precision-critical applications requiring real-time responsiveness, such as telecommunications network optimization or nowcasting the use of locally derived refractivity is strongly recommended. The identified performance gap during volatile periods underscores an opportunity to enhance climatological propagation models by integrating higher-resolution temporal data or localized calibration. Temporal refractivity analyses over Kaduna reinforce the need for high-resolution, meteorology-based refractivity datasets to improve propagation planning, especially for dynamic tropical environments [45].

Crucially, this work moves beyond a technical comparison to offer fundamental climatological insight. The observed refractivity patterns are explicitly linked to the phases of the West African monsoon, with distinct regimes associated with the dry Harmattan northeasterlies and the moist southwesterly monsoon flow. This connection not only validates the physical accuracy of the local sensor data but also frames continuous refractivity monitoring as a valuable proxy for understanding regional thermodynamic dynamics. The successful deployment of the low-cost, automated GSM-RC system establishes a practical and scalable method for advancing such integrated propagation and climate studies across West Africa.

Author Contributions

Conceptualization, A.B.G. and J.S.O.; methodology, A.B.G.; software, A.B.G.; validation, J.S.O., A.B.G. and O.V.O.; formal analysis, J.S.O. and A.B.G.; investigation, A.B.G.; resources, A.B.G., O.V.O. and W.A.T.; data curation, A.B.G. and W.A.T.; writing—original draft preparation, A.B.G.; writing—review and editing, J.S.O.; visualization, A.B.G, O.V.O. and W.A.T.; supervision, J.S.O.; project administration, A.B.G. and W.A.T.; funding acquisition, A.B.G, O.V.O. and W.A.T. All authors have read and agreed to the published version of the manuscript.

Funding

This research received no external funding.

Institutional Review Board Statement

Not applicable. This study did not involve humans or animals.

Informed Consent Statement

Not applicable.

Data Availability Statement

The data presented in this work is readily available upon request.

Conflict of Interest

All authors declare no conflict of interest in this paper.

References

[1] Yusuf, N., Ekpe, O.E., Said, R.S., et al., 2019. Seasonal and diurnal trends of surface refractivity in a tropical environment using ground-based automatic weather stations. Meteorology and Atmospheric Physics. 132, 327–340. DOI: https://doi.org/10.1007/s00703-019-00693-6

[2] Viher, M., Kos, T., Markezic, I., 2011. A study of the maximal height for the exponential model of the refractivity Index vertical profile in the Republic of Croatia. In Proceedings of the 53rd International Symposium Electronics in Marine (ELMAR), Zadar, Croatia, 14–16 September 2011; pp. 187–190.

[3] Viher, M., Prtenjak, M.T., 2012. A multi-year study of radio-wave refractivity profiles above the Adriatic Sea up to an altitude of 40 km. Meteorologische Zeitschrift. 21(4), 365–370.

[4] Jacques, P., Boudjabi, C., Besson, C.L., et al., 2012. Errors caused by long-term drifts of magnetron frequencies for refractivity measurement with a radar: Theoretical formulation and initial validation. Journal of Atmospheric and Oceanic Technology. 29(10), 1428–1434.

[5] Oyinloye, J.O., 1987. The troposphere in tropical and sub-tropical latitudes. In: Mitra, A.P., Reddy, B.M., Radicella, S.M., et al. (Eds.). Handbook on Radio Prop-

agation for Tropical and Sub-tropical Countries. URSI Committee on Developing Countries:Ghent, Belgium.

[6] Oyedum, O.D., Gambo, G.K., 1994. Surface radio refractivity in northern Nigeria. Nigerian Journal of Physics. 6, 36–41.

[7] Falodun, S.E., Kolawale, L.B., 2000. Studies of super-refractivity and ducting of radio waves in Nigeria. Nigerian Journal of Applied Physics. 1(1), 5–10.

[8] Adeyemi, B., Ewetumo, T., 2006. Intra-layer (low level/upper layer) refractivity relations over Lagos and Kano. Global Journal of Pure and Applied Sciences. 12(3), 403–408.

[9] Adeyemi, R.A., Kolawale, L.B., 1992. Seasonal and Diurnal Variations of Surface Refractivity in Akure, South-Western Nigeria [Master's Thesis]. Department of Physics, Federal University of Technology Akure: Akure, Nigeria.

[10] Tanko, M.M., Liman, M.S., Lumbi, W.L., et al., 2022. Spatial and seasonal estimation of tropospheric radio refractivity in Nigeria. African Scientific Reports. 1(1), 48–59. DOI: https://doi.org/10.46481/asr.2022.24

[11] Ladan, M.B., Oyedum, O.D., Jibrin, A.Y., et al., 2021. Study of seasonal surface refractivity over north central Nigeria. Physics Access. 1(2), 5–13.

[12] Falodun, S.E., 2004. Experimental Studies of Super-Refraction of the Microwave Signal [PhD Thesis]. Department of Physics, Federal University of Technology Akure: Akure, Nigeria.

[13] Falodun, S.E., Ajewole, M.O., 2006. Radio refractive index in the lowest 100-m layer of the troposphere in Akure, south western Nigeria. Journal of Atmospheric and Solar-Terrestrial Physics. 68(2), 236–243.

[14] Kolawale, L.B., Owonubi, J.J., 1982. The surface radio refractivity over Africa. Nigerian Journal of Science. 16(1–2), 441–454.

[15] Viher, M., 2006. A study of the modified refraction indices over the Alpine and sub-Alpine region. Meteorologische Zeitschrift. 15(6), 625–630.

[16] Viher, M., Prtenjak, M.T., Grisogono, B., 2013. A multi-year study of the anomalous propagation conditions along the coast of the Adriatic Sea. Journal of Atmospheric and Solar-Terrestrial Physics. 97, 75–84. DOI: https://doi.org/10.1016/j.jastp.2013.01.014

[17] Zungeru, M., Ahmed, M.S., Doko, G.M., et al., 2014. Modelling and development of a frequency modulated field strength indicator. International Journal of Emerging Trends in Engineering and Development. 1(4), 192–205.

[18] Giwa, A.B., Ewetumo, T., Ojo, J.S., et al., 2024. Development of a GSM-RC automated device for measuring mobile communication signal strength and meteorological parameters. Advance in Science, Technology and Engineering Systems Journal. 9(1), 149–164.

[19] Onawumi, K.C., Adetunji, E.O., 2025. Application of machine learning for radio refractivity prediction across climatic zones in West Africa. Current Journal of Applied Science and Technology. 44(8), 121–137.

[20] Ukhurebor, K.E., Nwankwo, W., 2020. Estimation of the refractivity gradient from measured essential climate variables in Iyamho-Auchi, Edo State, South-South Region of Nigeria. Indonesian Journal of Electrical Engineering and Computer Science. 19(1), 276–284. DOI: https://doi.org/10.11591/ijeecs.v19.i1.pp276-284

[21] Bean, B.R., Dutton, E.J., 1968. Radio Meteorology. Dover Publications Inc: New York, NY, USA.

[22] Freeman, R.L., 2007. Radio System Design for Telecommunications. John Wiley & Sons Inc: Hoboken, NJ, USA.

[23] Valma, E., Tamošiūnaitė, M., Tamošiūnas, S., et al., 2010. Determination of radio refractive index using meteorological data. Elektronika ir Elektrotechnika. 10(106), 125–128.

[24] Ali, S., Malik, S.A., Alimgeer, K.S., et al., 2012. Statistical estimation of tropospheric radio refractivity derived from 10 years meteorological data. Journal of Atmospheric and Solar-Terrestrial Physics. 77, 96–103.

[25] Alam, I., Mufti,S.A.A., Shah, M.Y., 2016. The effect of refractivity on propagation at UHF and VHF frequencies. International Journal of Antennas and Propagation. 2016(1), 4138329.

[26] Ojo, J.S., Ajewole, M.O., Sarkar, S.K., 2008. Rain rate and rain attenuation prediction for satellite communication in Ku and Ka bands over Nigeria. Progress in Electromagnetics Research B. 5, 207–223.

[27] Ogunrayi, O.A., Akinseye, F.M., Goldberg, V., et al., 2016. Descriptive analysis of rainfall and temperature trends over Akure, Nigeria. Journal of Geography and Regional Planning. 9(11), 195–202.

[28] Ogunjo, S.T., Adediji, A.T., Dada, J.B., 2017. Investigating chaotic features in solar radiation over a tropical station using recurrence quantification analysis. Theoretical and Applied Climatology. 127(1), 421–427.

[29] Ayantunji, B.G., Okeke, P.N., Urama, J.O., 2011. Diurnal and seasonal variation of surface refractivity over Nigeria. Progress in Electromagnetics Research B. 30, 201–222.

[30] Okoro, O.N., Agbo, G.A., 2012. The effect of variation of meteorological parameters on the tropospheric radio refractivity for Minna. Global Journal of Science Frontier Research Physics and Space Science. 12(2), 36–41.

[31] Falade, J.A., Adesanya, S.O., Akinyemi, G.A., 2014. Variability of meteorological factors on surface index over Mowe, a coastal area in Nigeria. Indian Journal of Radio and Space Physics. 43(6), 355–361.

[32] Adediji, A.T., Ajewole, M.O., Ojo, J.S., et al., 2015. Influence of some meteorological factors on tropospheric radio refractivity over a tropical location in Nigeria. MAUSAM. 66(1), 123–128.

[33] Akpootu, D.O., Aminu, Z., Yusuf, A., et al., 2024. Investigation of tropospheric refractivity and relevant parameters using meteorological variables over Bauchi, Nigeria. FUDMA Journal of Sciences. 8(2), 306–314.

[34] Adediji, A.T., Rotimi, C.O., Ajayi, T.M., 2012. Influence of temperature and water vapour on surface refractivity in Akure, south-western Nigeria. Journal of Science and Technology. 3(2), 32–43.

[35] Okoro, O.N., Agbo, G.A., Ekpe, J.E., et al., 2013. Comparison of hourly variations of radio refractivity for quiet and disturbed days during dry and rainy seasons at Minna. International Journal of Basic and Applied Sciences. 2(1), 58–63.

[36] Ojo, O.L., Ajewole, M.O., Adediji, A.T., et al., 2014. Microwave anomalous propagation conditions in the first 100-m altitude in a tropical location. Journal of Microwave Power and Electromagnetic Energy. 48(2), 131–137.

[37] Bello, G., Akpootu, D.O., Zoramawa, A.B., et al., 2024. Performance analysis of tropospheric radio refractivity along with refractivity gradient and effective Earth radius in the coastal zone of Nigeria. UMYU Scientifica. 3(3), 251–266.

[38] Wang, S., Lim, T.H., Oh, K., et al., 2021. Prediction of wide range two-dimensional refractivity using an IDW interpolation method from high-altitude refractivity data of multiple meteorological observatories. Applied Sciences. 11(4), 1431.

[39] Emetere, M.E., Akinwumi, O.A., Omotoso, T.V., et al., 2015. A tropical model for analyzing radio refractivity in selected locations in north central Nigeria. In Proceedings of the 2015 International Conference on Space Science and Communication (Iconspace), Langkawi, Malaysia, 10–12 August 2015; pp. 1–3.

[40] Yusuf, B.L., Joseph, B.D., 2023. Comparative Analysis of Surface Refractivity Variations in the Sahel and Coastal Zones of Nigeria. American Journal of Electrical and Computer Engineering. 7(1), 10–18.

[41] Onawumi, K.C., Adediji, A.T., Ogunjo, S.T., 2025. Machine learning-based surface refractivity prediction in coastal and inland regions of West Africa: A comparative study. In Proceedings of the 8th URSI-NG Annual Conference (URSI-NG 2024). Atlantis Press: Paris, France. pp. 213–223.

[42] Sakkas, A., Christofilakis, V., Lolis, C.J., et al., 2024. Harnessing the radio frequency power level of cellular terminals for weather parameter sensing. Electronics. 13(5), 840. DOI: https://doi.org/10.3390/electronics13050840

[43] Durodola, O.M., Samuel, O.E., Nnaike, D.O., et al., 2025. Seasonal modelling of radio refractivity in Jos, Nigeria. In Proceedings of the 8th URSI-NG Annual Conference (URSI-NG 2024). Atlantis Press: Paris, France. pp. 189–198.

[44] Akinbolati, A., Abe, O.E., 2026. Evaluation of ITU-R refractivity models for predicting atmospheric refractivity over West Africa. Radio Science. 61(1), e2025RS007845.

[45] Sabiru, A.Y., Akinbolati, A., Ikechiamaka, F.N., 2025. Temporal analysis of radio refractivity variation over Kaduna: Implications for radio wave systems. UMYU Scientifica. 4(2), 100–108.